Article

Chinese Science Bulletin

SPECIAL ISSUE: New Energy Materials

November 2012 Vol.57 No.32: 4181–4187
doi: 10.1007/s11434-012-5417-3

Ce-doped $LiNi_{1/3}Co_{(1/3-x/3)}Mn_{1/3}Ce_{x/3}O_2$ cathode materials for use in lithium ion batteries

ZHANG YingJie[1,2], XIA ShuBiao[1,3*], ZHANG YanNan[1], DONG Peng[1], YAN YuXing[1,3]& YANG RuiMing[1,3]

[1] *Faculty of Material Science and Engineering, Kunming University of Science and Technology, Kunming 650093, China;*
[2] *Key Laboratory of Ethnic Medicine Resource Chemistry, State Ethnic Affairs Commission & Ministry of Education, Yunnan University of Nationalities, Kunming 650031, China;*
[3] *Faculty of Chemistry & Chemical Engineering, Qujing Normal University, Qujing 655011, China*

Received May 14, 2012; accepted June 27, 2012

$LiNi_{1/3}Co_{1/3}Mn_{1/3}O_2$ and Ce-doped $LiNi_{1/3}Co_{1/3}Mn_{1/3}O_2$ cathode materials were synthesized by a co-precipitation method and solid phase synthesis and characterized using X-ray diffraction (XRD) and scanning electron microscopy (SEM). The results indicated that the resultant cathode materials with different Ce content all had a good layer structure and high crystallinity. Electrochemical performance testing of the cathode materials showed that the discharge capacity increased with increasing Ce content while the initial reversible capacity attenuation decreased with Ce doping. When the Ce content of the cathode materials is x=0.2, and the current charge and discharge rate is a constant 0.2 C, the discharge capacity maintained 91% of its initial capacity after cycling 50 times.

lithium ion batteries, cathode materials, $LiNi_{1/3}Co_{1/3}Mn_{1/3}O_2$

Citation: Zhang Y J, Xia S B, Zhang Y N, et al. Ce-doped $LiNi_{1/3}Co_{(1/3-x/3)}Mn_{1/3}Ce_{x/3}O_2$ cathode materials for use in lithium ion batteries. Chin Sci Bull, 2012, 57: 4181–4187, doi: 10.1007/s11434-012-5417-3

The development of lithium ion batteries is important to improve both energy efficiency of such devices and their impact on the environment. Research to develop positive materials for such application is of major importance. To date, $LiCoO_2$ has been the most successful cathode material developed and applied to commercial lithium ion batteries. However, because of its high price, toxicity, and actual discharge capacity being half that of the theoretical capacity, the use of $LiCoO_2$ in batteries has been restricted [1]. So, the identification of new cathode materials that are low-cost, and have a large reversible capacity, a high voltage, a stable structure, and are environmentally friendly, is the main focus of future research [2]. Aside from $LiCoO_2$, other positive materials such as $LiMn_2O_4$ (spinel structure), $LiFePO_4$ (olivine structure) and $LiNi_{1/3}Co_{1/3}Mn_{1/3}O_2$ all have their advantages and disadvantages [3]. $LiMn_2O_4$ comprises channels having a three-dimensional structure to enable lithium ions to undergo intercalation and demineralization, and affording this material with such advantages as a higher discharging voltage, low cost, and environmentally friendly. However, $LiMn_2O_4$ also has a lower reversible capacity and the Jahn-Teller effect occurs at high temperature to damage the active material structure [4]. $LiFePO_4$ has been the main driving force for the most popular battery materials in recent years, but its low electronic conductivity and low actual discharge capacity highlights the limitations of this material in business applications [5–7].

$LiNi_{1/3}Co_{1/3}Mn_{1/3}O_2$ is the most likely alternative to $LiCoO_2$ for use as the cathode in commercial lithium ion batteries. $LiNi_{1/3}Co_{1/3}Mn_{1/3}O_2$ has the same layer structure as $LiCoO_2$ and the same features as the corresponding Ni, Co, Mn [8,9]. But, $LiNi_{1/3}Co_{1/3}Mn_{1/3}O_2$ also has the problems of a low-rate capacity, a low-tap density, a low-electronic conductivity, and cation mixing, which are all required to be solved. At present, research into the improvement of the performance of the cathode materials has mainly

*Corresponding author (email: xiashubiao401@163.com)

focused on two methods: the surface coating method and ion doping. Surface coating of the positive materials has mainly been achieved using metal oxides (ZnO, Al_2O_3, ZrO_2, TiO_2, SiO_2, etc.) to protect the positive materials from being dissolved in the electrolyte and other side reactions [10]. Doping of the positive materials has mainly been achieved using Ti, Fe, Cr, Zn, Mg, etc. to stabilize the structure of the positive material layer, and reduce cation mixing [3,11]. Rare earth metals with excellent photo-electromagnetic effects can form composites with many materials to form new materials with enhanced performance [12]. Ha et al. [13,14] systematically researched the electrochemical performance and cyclic life of the positive materials by coating of the positive materials CeO_2 . Wang et al. [15] modified $LiNi_{1/3}Co_{1/3}Mn_{1/3}O_2$ by coating it with 1.0 wt% CeO_2 using a 20 mA/g current density. The resulting discharge capacity of the Ce doped $LiNi_{1/3}Co_{1/3}Mn_{1/3}O_2$ reached 182.5 mAh/g. It is our understanding that studies of the Ce doping of positive materials have yet to be reported. So, this paper focuses on the Ce doping of positive materials to understand its influence of the properties of the positive material.

1 Experimental

1.1 Material composition

$LiNi_{1/3}Co_{1/3}Mn_{1/3}O_2$ powder was synthesized by a co-precipitation method using the following pristine materials. LiOH, $NiSO_4 \cdot 6H_2O$, $CoSO_4 \cdot 7H_2O$, $MnSO_4 \cdot H_2O$, NaOH, $NH_3 \cdot H_2O$, $Ce(NO_3)_3$ are from Kermel, China.

The co-precipitation reactions used stoichiometric amounts of $NiSO_4$, $MnSO_4$, $CoSO_4$ and $Ce(NO_3)_3$ as the starting materials according to the formula $LiNi_{1/3}Co_{(1/3-x/3)}Mn_{1/3}Ce_{x/3}O_2$. The hybrid solution was slowly added dropwise into a NaOH solution while maintaining a constant temperature of 60°C. Ammonia water was then added to the solution to achieve a pH value of 11, followed by stirring for 2 h. The reaction products were separated from the solution using a suction filter and washed with deionized water, until a pH value close to neutral. The precipitate was dried at 110°C under vacuum for 12 h to obtain the precursor, $Ni_{1/3}Co_{1/3}Mn_{1/3}(OH)_2$. According to the formula, $LiNi_{1/3}Co_{(1/3-x/3)}Mn_{1/3}Ce_{x/3}O_2$, the ratio of Li^+:M^{4+} would be 1.03:1. To this was added LiOH and the precursor, and the mixture ground in a crucible, and heated in a box fritting furnace (KSL1700X; Hefei Kejing Materials Technology Co. Ltd., China). The mixture was first heated for 8 h at 450°C, then calcined at 880°C for 20 h, and finally cooled to room temperature.

1.2 Measurements

XRD diffraction measurements of the as-prepared $LiNi_{1/3}Co_{(1/3-x/3)}Mn_{1/3}Ce_{x/3}O_2$ materials were carried out using a Rigaku D/MAX-2500 instrument with $CuK_{\alpha 1}$ radiation. The particle morphology of the sampled powders was obtained by scanning electron microscopy (SEM) using a Philips XL-30 (emission voltage 25 kV) microscope. Electrochemical measurements of the cathode electrode were carried out using a CR2025 type coin cell. The active materials, binder (PVDF), and conductive material (acetylene black AB) were mixed in a weight ratio of $LiNi_{1/3}Co_{1/3}Mn_{1/3}O_2$/PVDF/AB=84∶8∶8. The obtained material was subsequently dried at 120°C for 12 h in a vacuum. Li metal was used as the negative electrode; Celgard 2500 was used as a diaphragm with a thickness of 25 μm. The electrolyte solution comprised 1 mol/L of $LiPF_6$ dissolved in EC∶DMC∶DEC= 1∶1∶1 (Zhang Jiagang Guo Tai Hua Rong Corp., Ltd., China). R2025-type coin cells were assembled in an argon-filled glove box (Nanjing MIKROUNA 2440/750). The battery test system used was LAND-CT2001A. Circulation current-voltage tests were carried out using a ShangHai ChenHua 660C electrochemical workstation. The electrode system comprised a working electrode, a counter electrode and a reference electrode. Scan frequency ranged from 1 to 0.01 MHz, and Sine wave amplitude was 5 mV; scan rates used were 0.1, 0.2, 0.5 mV/s, at a scanning voltage range from 2.5 to 4.2 V.

2 Results and discussion

2.1 XRD analysis

X-ray powder diffraction patterns of the four as-prepared compounds are shown in Figure 1. As $LiCoO_2$, $LiNi_{1/3}Co_{1/3}Mn_{1/3}O_2$ have layer structures with a space group of R-3m [16,17], all the diffraction peaks of the four XRD patterns can be indexed to a good layer structure and high crystallinity. The clear splitting of the 108/110 and 006/102 peaks, which were in good agreement with that reported previously, and compared well with the $LiCoO_2$ standard diffraction patterns; all of the diffraction peaks except (003) exhibit a slight shift, which is ascribed to the addition of nickel and manganese to the cathode materials. It is clearly seen that the new peak appeared after Ce doping. Furthermore, the other peak is consistent with the standard peak of CeO_2, while the other peaks are consistent with pure $LiNi_{1/3}Co_{1/3}Mn_{1/3}O_2$. This result shows that Ce doping does not change the basic $LiNi_{1/3}Mn_{1/3}Co_{1/3}O_2$ crystal structure. The lattice constant was obtained following an XRD refinement (Table 1). As the quantity of Ce-doping for x=0.1, the value of a suddenly increased and c decreased, which would explain the existence of trace amounts of Ce^{4+} doping in the lattice. Although it is hard to form a solid solution comprising Ce^{3+} (r=0.102 nm), Ni^{3+} (r=0.056 nm), Mn^{3+} (r=0.068 nm) and Co^{3+} (r=0.054 nm), Ce^{4+} (r=0.087 nm) can form a solid solution in sintering trace, and caused a sudden increase in the value of the lattice parameters [18–20]. CeO_2 was also observed coated on the surface of the particles. When the

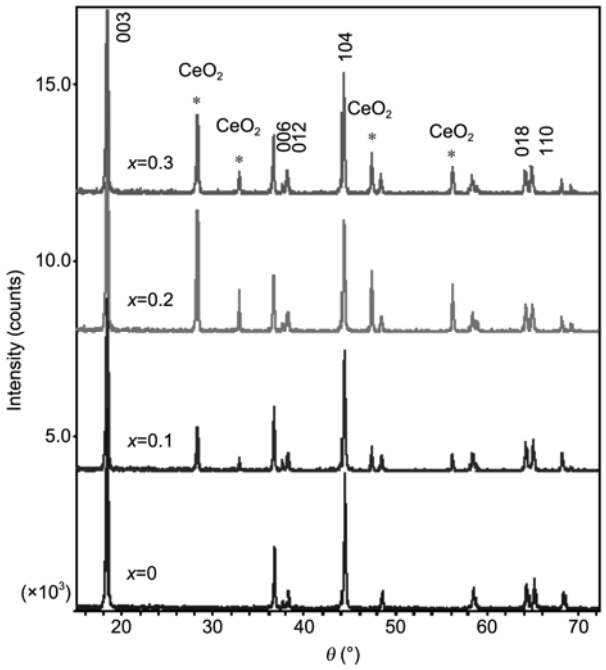

Figure 1 XRD patterns of four $LiNi_{1/3}Co_{(1/3-x/3)}Mn_{1/3}Ce_{x/3}O_2$ samples.

Table 1 The lattice parameter of four $LiNi_{1/3}Co_{(1/3-x/3)}Mn_{1/3}Ce_{x/3}O_2$

	a (Å)	c (Å)	c/a	I_{003}/I_{104}	V (Å^3)
x=0	2.8557(3)	14.2534(1)	4.991(1)	1.453	100.67
x=0.1	2.8773(5)	14.2128(9)	4.939(6)	1.443	101.91
x=0.2	2.8660(6)	14.2522(5)	4.972(8)	1.805	101.39
x=0.3	2.8681(8)	14.2459(7)	4.966(9)	1.529	101.49

Ce doping was increased for the cathode material (x=0.2), the mixing of Ni^{2+} and Li^+ ions in the 3a position caused oxidation of the Ni^{2+} ions to Ni^{3+} as a result of the strong oxidation capability of Ce^{4+}, because of the ion radius of Ni^{3+} being smaller than that of Ni^{2+} (r=0.064 nm), so the value of a decreased, while c/a increased and would be suppressed.

In addition, the ratio of the $I_{003}:I_{104}$ revealed the extent of the cation mixing, as the doping quantity was x=0.2, the ratio of the $I_{003}:I_{104}$ reaches 1.805. When doping amount to further x=0.3, Ce^{4+} cannot dope to the lattice. Table 1 shows the lattice constant change is very small, so the Ce-doping would be as more as CeO_2 coated in particle surface [21,22]. From the expanded views of the 003 peak and the 104 peak in Figure 2, we find that the 2θ value of the 003 peaks migrated to high angles with increasing quantity of Ce doping. The largest high angle migration occurred when x=0.2. The 003 peak reflects the $2d$ layer structure; according to the formula, $2d\sin\theta=n\lambda$, the 2θ offset to high angles reflects the reduction of the d value. The ion radius of the larger Ce^{4+} ions enabled the Ce^{4+} ion to be doped into the 3b position,

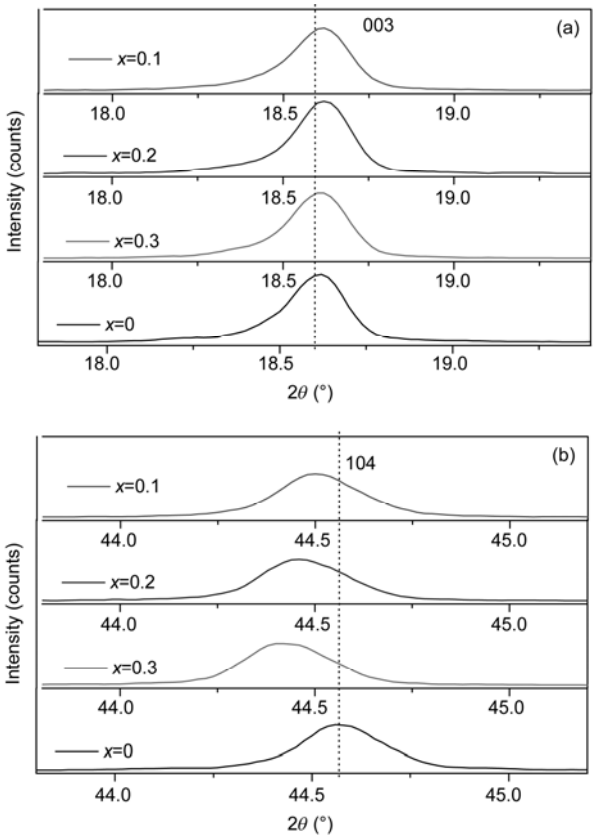

Figure 2 The expanded views of the 003 peak (a) and 104 peak (b) of four $LiNi_{1/3}Co_{(1/3-x/3)}Mn_{1/3}Ce_{x/3}O_2$.

leading to an increase in the size of the octagonal MO_6. On the other hand, the 2θ values of the 104 peaks have a small angle migration. The 104 peak reflects the $2d$ layer structure and cubic rock salt structure, so the 104 peak small angle migration caused by the amount of cubic rock salt structure would be reduced, and the cation mixing would be suppressed [23,24].

2.2 SEM analysis

SEM images of the $LiNi_{1/3}Co_{(1/3-x/3)}Mn_{1/3}Ce_{x/3}O_2$ powders with different quantities of doped Ce are shown in Figure 3. It can be seen from the graph that Ce doping had a certain effect on the morphology of the $LiNi_{1/3}Co_{1/3}Mn_{1/3}O_2$ cathode material. Prior to Ce doping, the surface of the particles was relatively bright and clean. However, the surface roughness of the particles was observed to increase with increased Ce doping, in which some of the flow material covered the particle surface. A combined SEM and XRD analysis confirmed that the flocculant coating on the particle surface is CeO_2. It was found that the quantity of flocculant increased with Ce doping. Indeed, when x=0.3, the quantity of flocculant is at a maximum, as determined by SEM observation. This phenomenon is expected to influence the Li^+ intercalation and demineralization process.

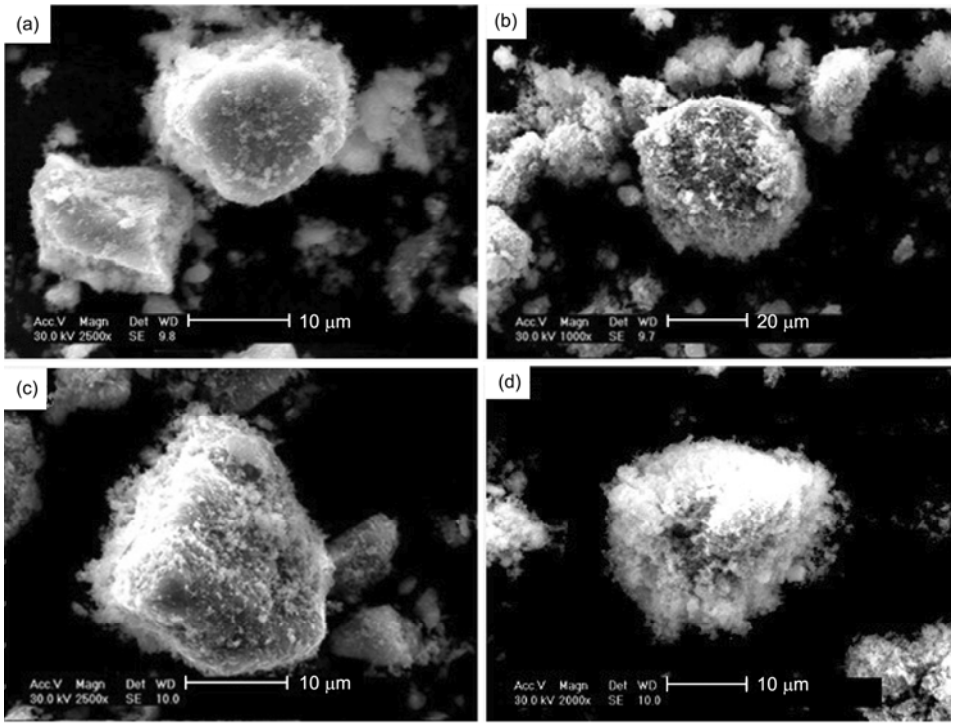

Figure 3 SEM image of four $LiNi_{1/3}Co_{(1/3-x/3)}Mn_{1/3}Ce_{x/3}O_2$. (a) x=0; (b) x=0.1; (c) x=0.2; (d) x=0.3.

2.3 Electrochemistry analysis

Cyclic-voltammetry (CV) is a conventional electrochemical method used to analyze the mass transfer process of an electrode and a nearby solution interface.

The CV test used to study the assembled lithium-ion batteries was based on a two electrode system. The working electrode used was a LIB cathode material, while the counter electrode and the reference electrode were both fabricated from metallic lithium. The scanning frequency range used was from 1 to 0.01 MHz, with a sine wave amplitude of 5 mV, and scan rates of 0.1, 0.2, and 0.5 mV/s. The scanning voltage used ranged from 2.6 to 4.2 V, working at normal temperature.

Figure 4 shows the CV curves of the following cathode materials, $LiNi_{1/3}Co_{(1/3-x/3)}Mn_{1/3}Ce_{x/3}O_2$ (x=0, x=0.1, x=0.2, x=0.3), obtained by scanning at a rate of 0.1 mV/s. It can be seen from the graph that the reduction peak for each of the cathode materials has a small number of deflections remaining as a result of the increased Ce-doping. The reduction peak for the pure materials is observed at 3.718 V, and then from 3.680 V (x=0.1) deflection to 3.637 V (x=0.3) after doping with Ce. When x=0.1, the peak point current dropped, while the amount of Ce doping increased to x=0.2, x=0.3 the peak current increased slightly. This suggests that the electronic conductivity of the cathode materials improved as the amount of Ce doping increased to a certain amount. The voltage interval of the peak point current in the pure cathode materials is 0.201 V, and subsequently increased to 0.379 V when x=0.3. This result suggests that the electrode

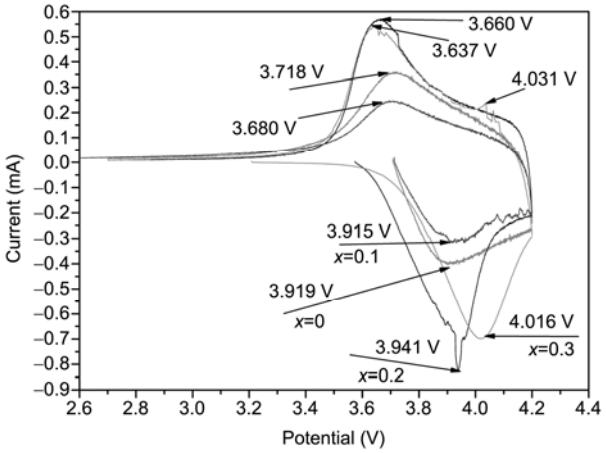

Figure 4 Cyclic voltammogram of samples doped and undoped with Ce.

polarization has increased and the degree of reversibility was affected [25].

For a series of reaction diffusions, the diffusion process is typically controlled by the diffusion speed, on account of it being the slowest, or rate determining step. Ideally, the diffusion process in lithium ion batteries should principally be controlled by a solid process. The positive point peak current of a reversible system can be expressed by the Randles-Sevick equation:

$$I_p = 2.69\times10^5 An^{3/2} D_o^{1/2} v^{1/2} C_o . \quad (1)$$

In eq. (1), I_p is the peak current, A is the electrode area; n is

the number of electrons; D is the diffusion coefficient, cm^2/s; v is the scanning speed, v/s; and C is the concentration, mol/L. Based on formula (1) for the diffusion control electrode reaction, we can calculate the diffusion equation under the condition of the semi-infinite diffusion. We can calculate the lithium ion diffusion coefficient in both the liquid and solid phase, which imparts significant meaning to research of the lithium ion electrode reaction process [26].

For this experiment, A=0.5 cm^2, n=1. If we want to calculate D_s (diffusion coefficient in solid phase), we must first calculate C_0. There are 13 lithium ions for each $LiNi_{1/3}Co_{1/3}Mn_{1/3}O_2$ unit cell. The volume of the unit cell is 101.3 $Å^3$, so the concentration can be calculated as $C_0=2.15\times10^{-1}$ mol/L. When a lithium ion emerges from the unit cell, the concentration falls to $C_0'=1.98\times10^{-1}$ mol/L.

We can use different scanning speeds to test the characteristics of the peaks shown in Figure 4 and map the I_p-$v^{1/2}$ relationship, where I_p-$v^{1/2}$ has a good linear relationship. The results are shown in Figure 5. It can be seen from Table 2 that Ce doping has a certain effect on the diffusion coefficients in the solid phase. In the solid phase, only traces of Ce doping would be evident in the crystal structure, because of the larger radius of the Ce^{4+} ion. Additional Ce doping mainly occurs as a CeO_2 coating on the particle surface. As a result, the additional Ce doping suppresses the migration of lithium ions to the interface. With the increased Ce doping, the quantity of Ce doped into the lattice increased, making the Ni^{2+} ions, which are mixed in the Li^+ 3a position, undergo oxidation to forms Ni^{3+} ions and back to its 3b position, because of the strong oxidizing capability of the Ce^{4+} ion, which increases the lithium ion diffusion ability [27].

Figure 6 shows the difference of the $LiNi_{1/3}Co_{(1/3-x/3)}Mn_{1/3}Ce_{x/3}O_2$ impedance change after the initial cycle. Liu et al. [28], Zhuang et al. [29] and Lee et al. [30] considered that the high-to-medium frequency semicircle was attributed to the resistance of the surface film (R_{sf}) covered electrode

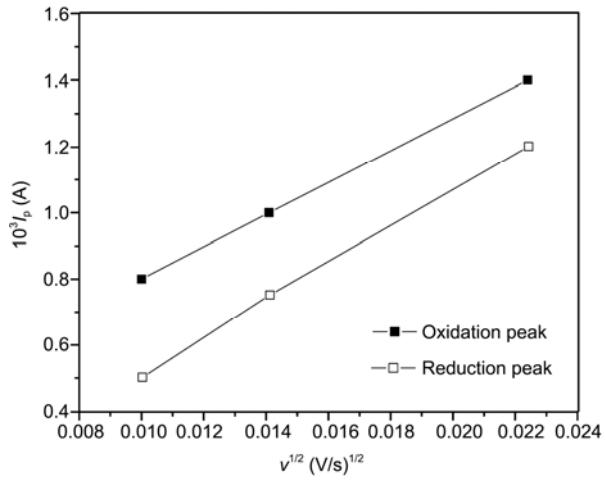

Figure 5 Dependence of peak currents on the square root of potential scan rates of different region.

Table 2 The chemical diffusion coefficient for $LiNi_{1/3}Co_{(1/3-x/3)}Mn_{1/3}Ce_{x/3}O_2$

State	Composition	D_s (cm^2/s)
Charge	x=0	1.575×10^{-12}
	x=0.1	7.122×10^{-13}
	x=0.2	3.872×10^{-12}
	x=0.3	3.539×10^{-12}
Discharge	x=0	2.371×10^{-12}
	x=0.1	1.458×10^{-12}
	x=0.2	9.597×10^{-12}
	x=0.3	7.007×10^{-12}

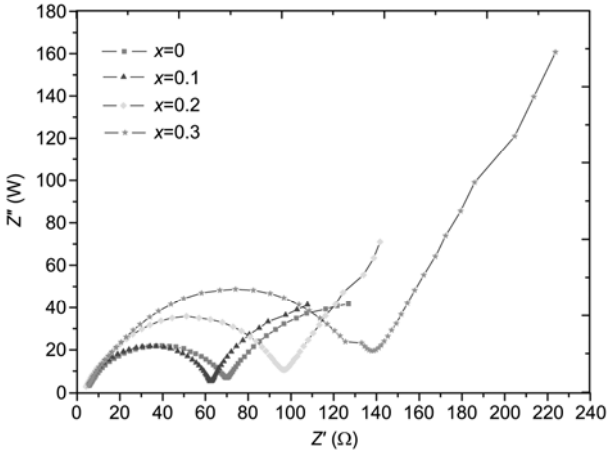

Figure 6 The impedance change of four $LiNi_{1/3}Co_{(1/3-x/3)}Mn_{1/3}Ce_{x/3}O_2$ after initial cycle.

particles, and the low-frequency was attributed to the charge transfer resistance (R_{ct}) at the interface between the electrode and the electrolyte in the impedance Nyquist picture. As can be seen from Figure 5, after the initial cycle, the surface impedance (R_{sf}) increased with increasing amounts of Ce doping. The R_{sf} value of the undoped $LiNi_{1/3}Co_{(1/3-x/3)}Mn_{1/3}Ce_{x/3}O_2$ increased from 60 to 140 Ω as the doping quantity x=0.3 after the initial cycle. It shows that the surface of the CeO_2 blocks the Li^+ intercalation and demineralization, and the block role would be increased with increasing Ce-doping, which is also verified by the results of the XRD and SEM analyses.

2.4 Circulation performance analysis

Figure 7 compares the initial charge-discharge curves of $LiNi_{1/3}Co_{(1/3-x/3)}Mn_{1/3}Ce_{x/3}O_2$ (x=0, x=0.1, x=0.2, x=0.3) with a current density of 28 mAh/g (0.2 C rate) between 2.7–4.2 V. When x=0, the discharge capacity is about 110 mAh/g which is less than that in [8,9,15]. This is due to the individual 4.2 V cut-off voltage, and the relatively high current density, which will increase the electrode polarization, and influence the electrode performance. In addition, synthetic

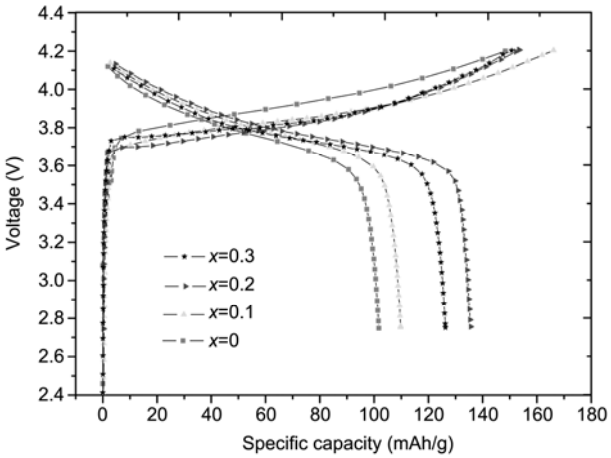

Figure 7 Charge/discharge curves of the initial cycle for $LiNi_{1/3}Co_{(1/3-x/3)}Mn_{1/3}Ce_{x/3}O_2$ samples in 0.2 C.

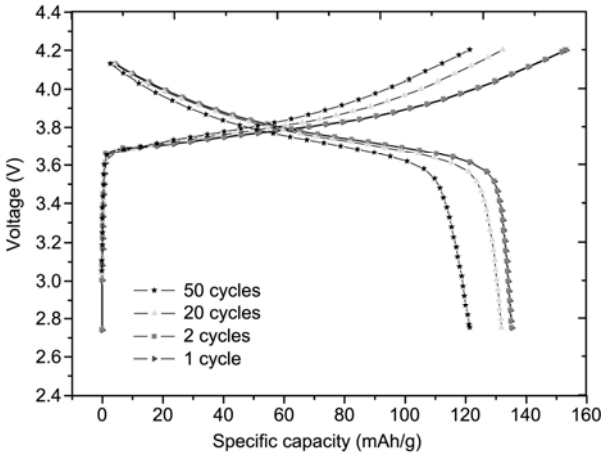

Figure 8 Charge/discharge curves of $LiNi_{1/3}Co_{(1/3-x/3)}Mn_{1/3}Ce_{x/3}O_2$ samples (x=0.2) in 0.2 C.

materials have larger particles, which would have an effect on the discharge capacity. But the recession of the reversible capacity was significantly reduced after doping the material with a small amount of rare earth cerium. When x=0.2, the discharge capacity was observed to be close to 140 mAh/g, and the reduction of reversible capacity was 8.5% (first cycle), which was obviously lower than the loss of the pure materials.

To evaluate the cycling behavior at different quantities of Ce doping, conditions of up to 50 cycles were performed, at a charge rate of 1 C. The discharge capacity of $LiNi_{1/3}Co_{(1/3-x/3)}Mn_{1/3}Ce_{x/3}O_2$ shows very good capacity retention. When x=0.2, as one can observe in Figure 8, the second cycle curves were overlapped with the first ones, where the discharge capacity reached a value of 132 mAh/g and maintained a capacity of 98% during the first 20 cycles, and then reached a value of 121 mAh/g and maintained a capacity of 91%, after 50 cycles.

Figure 9 shows the circular curves achieved for the $LiNi_{1/3}Co_{(1/3-x/3)}Mn_{1/3}Ce_{x/3}O_2$ cathode materials when x=0 and x=0.2, taken at a charge rate of 0.2 C and a discharge capacity of 28 mAh/g. When x=0, the materials maintained a capacity of 86% after 50 cycles; when x=0.2, the materials maintained a capacity of 91% for 121 mAh/g. So, doping the cathode materials with an appropriate amount of Ce may optimize the structure of $LiNi_{1/3}Co_{(1/3-x/3)}Mn_{1/3}Ce_{x/3}O_2$ and prevent the active elements from separating out from the surface of the positive material, as well as suppressing the cation mixing, thereby increasing the discharge capacity and improving the material circulation ability.

Figure 10 shows the cycling abilities of the $LiNi_{1/3}Co_{(1/3-x/3)}Mn_{1/3}Ce_{x/3}O_2$ cathode materials (x=2) under different rates, in which the discharge capacity at a low or high rate shows excellent capacity retention. The discharge capacity maintains a value of 98% at a charge rate of 0.2 C, and more than 95% at a charge rate of 1 C, after 20 cycles under normal temperature.

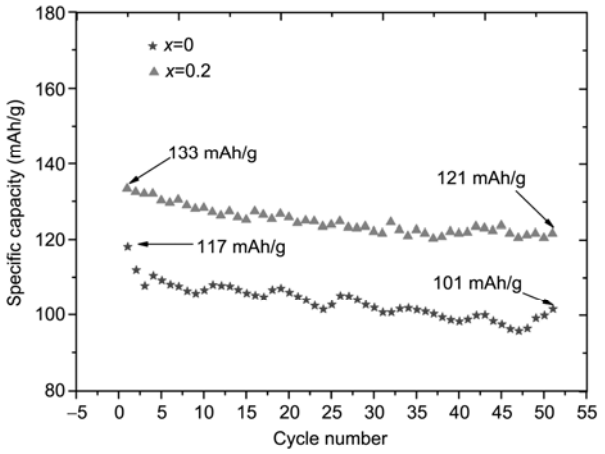

Figure 9 Cycle abilities of $LiNi_{1/3}Co_{(1/3-x/3)}Mn_{1/3}Ce_{x/3}O_2$ samples in 0.2 C (x=0, x=0.2).

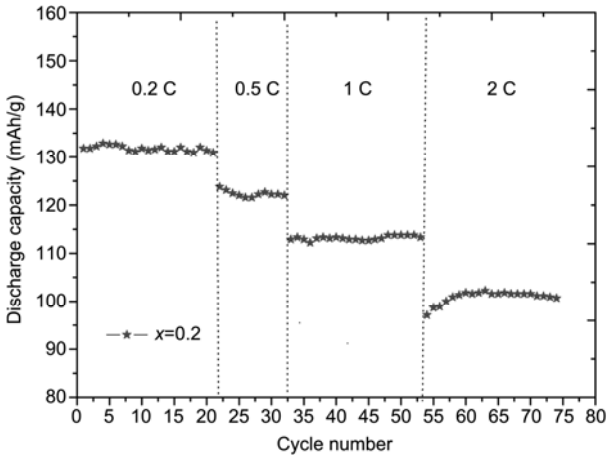

Figure 10 Cycle abilities of $LiNi_{1/3}Co_{(1/3-x/3)}Mn_{1/3}Ce_{x/3}O_2$ in different current rate (x=0.2).

3 Conclusion

(1) $LiNi_{1/3}Co_{(1/3-x/3)}Mn_{1/3}Ce_{x/3}O_2$ was prepared by a co-

precipitation method and solid phase synthesis with a good layer α-$NaFeO_2$ structure. The cerium in $LiNi_{1/3}Co_{(1/3-x/3)}Mn_{1/3}Ce_{x/3}O_2$ was mainly formed as CeO_2 on the surface of the active material, together with a small amount of cerium ions doped into the lattice.

(2) In the case of $LiNi_{1/3}Co_{(1/3-x/3)}Mn_{1/3}Ce_{x/3}O_2$ cathode materials, when x=0.2, the electronic conductivity and the spread rate of the lithium ions are notably improved when compared with $LiNi_{1/3}Co_{1/3}Mn_{1/3}O_2$. Trace amounts of Ce^{4+} doping into the lattice were observed. Ce was also observed as CeO_2 coated on the surface of the particles of the $LiNi_{1/3}Co_{(1/3-x/3)}Mn_{1/3}Ce_{x/3}O_2$ cathode material.

(3) Doping cathode materials with cerium will stabilize the positive material layer structure, and suppress cation mixing. Such results are beneficial to reduce the recession of irreversible capacity for the initial cycle, and improve the discharge capacity and circulation lives of these materials. The $LiNi_{1/3}Co_{(1/3-x/3)}Mn_{1/3}Ce_{x/3}O_2$ cathode materials can also maintain good electrochemistry properties during high charge rates.

1 Bandhauer T M, Garimella S, Fuller T F. A critical review of thermal issues in lithium-ion batteries. J Electrochem Soc, 2011, 158: R1–R25
2 Choi N S, Lee Y, Kim S S. Improving the electrochemical properties of graphite/$LiCoO_2$ cells in ionic liquid-containing electrolytes. J Power Sources, 2010, 195: 2368–2371
3 Fergus J W. Recent developments in cathode materials for lithium ion batteries. J Power Sources, 2010, 195: 939–954
4 Lu D S, Li W S, Zuo X X. Study on electrode kinetics of Li^+ insertion in $Li_xMn_2O_4$ ($0\leqslant x\leqslant 1$) by electrochemical impedance spectroscopy. J Phys Chem C, 2007, 111: 12067–12074
5 Piana M, Cushing B L, Goodenough J B. A new promising sol–gel synthesis of phospho-olivines as environmentally friendly cathode materials for Li-ion cells. Solid State Ionics, 2004, 175: 233–237
6 Zhang D Y, Zhang P X, Lin M C. Property and structure of carbon-coated $LiFePO_4$. J Inorg Mater M, 2011, 26: 265–270
7 Padhi A K, Nanjundaswamy K S, Goodenough J B. Phospho-olivines as positive-electrode materials for rechargeable lithium batteries. J Electrochem Soc, 1997, 144: 1188–1194
8 Naoaki Y, Tsutomu O. Novel lithium insertion material of $LiCo_{1/3}Ni_{1/3}Mn_{1/3}O_2$ for advanced lithium-ion batteries. J Power Sources, 2003, 121: 171–174
9 Ohzuku T, Makimura Y. Layered lithium insertion material of $LiCo_{1/3}Ni_{1/3}Mn_{1/3}O_2$ for lithium-ion batteries. Chem Lett, 2001, 30: 642–643
10 Li D C, Kato Y, Kobayakawa K, et al. Preparation and electrochemical characteristics of $LiNi_{1/3}Mn_{1/3}Co_{1/3}O_2$ coated with metal oxides coating. J Power Sources, 2006, 160: 1342–1348
11 Ye N Q, Liu C J, Shen S Y. Drawbacks and improve ways of $LiNiO_2$ as a cathode material for lithium ion batteries. J Inorg Mater, 2004, 19: 1217–1224
12 Song X L, Qiu G Z, Qu P. Synthesis and performance of CeO_2 nanocrystallines by precipitation method. J Hunan Univ (Nat Sci), 2004, 31: 13–17
13 Ha H W, Yun N J, Kim M H, et al. Enhanced electrochemical and thermal stability of surface-modified $LiCoO_2$ cathode by CeO_2 coating. Electrochim Acta, 2006, 51: 3297–3302
14 Ha H W, Yun N J, Kim K. Improvement of electrochemical stability of $LiMn_2O_4$ by CeO_2 coating for lithium-ion batteries. Electrochim Acta, 2007, 52: 3236–3241
15 Wang M, Wu F, Su Y F. Coating-CeO_2 for $LiMn_{1/3}Co_{1/3}Ni_{1/3}O_2$ of Li-ion battery cathode material. Sci China Ser E, 2009, 39: 809–813
16 Ohzuku T, Ueda A, Nagayama M, et al. Comparative study of $LiCoO_2$, $LiNi_{1/2}Co_{1/2}O_2$ and $LiNiO_2$ for 4-volt secondary lithium cells. Electrochim Acta, 1993, 38: 1159–1167
17 Zhu X H, Chen N, Lian F. First principle calculation of lithiation/delithiation voltage in Li-ion battery materials. Chin Sci Bull, 2011, 56: 3229–3232
18 Cheng J M, Chob Y D, Hsiao C L, et al. Electrochemical studies on $LiCoO_2$ surface coated with $Y_3Al_5O_{12}$ for lithium-ion cells. J Power Sources, 2009, 189: 279–287
19 Naoaki Y, Kazuhiro Y, Seung-Taek M, et al. Detail studies of a high-capacity electrode material for rechargeable batteries, Li_2MnO_3-$LiCo_{1/3}Ni_{1/3}Mn_{1/3}O_2$. J Am Chem Soc, 2011, 13: 4414–4419
20 Chen Y C, Xu X J, Cui H Z. Preferred orientation of crystals and the intensity ratios of XRD peaks of cathode material $LiCoO_2$. Acta Phys–Chim Sin, 2007, 23: 1948–1953
21 Naoaki Y, Tsutomu O. Novel lithium insertion material of $LiCo_{1/3}Ni_{1/3}Mn_{1/3}O_2$ for advanced lithium-ion batteries. J Power Sources, 2003, 121: 171–174
22 Shaju K M, Subba R G V, Chowdari B V R. Performance of layered $LiNi_{1/3}Co_{1/3}Mn_{1/3}O_2$ as cathode for Li-ion batteries. Electrochim Acta, 2002, 48: 145–151
23 Hwang B J, Tsai Y W, Ceder G. A combined computation experimental study on $LiNi_{1/3}Co_{1/3}Mn_{1/3}O_2$. Chem Mater, 2003, 15: 3676–3682
24 Tsai Y W, Hwang B J, Ceder G. *In-situ* X-ray absorption spectroscopic study on variation of electronic transitions and local structure of $LiNi_{1/3}Co_{1/3}Mn_{1/3}O_2$ cathode material during electrochemical cycling. Chem Mater, 2005, 17: 3191–3199
25 Xiong X Q, Jiang Y, Xia S A, et al. Synthesis and modification of well-ordered layered cathode oxide $LiNi_{2/3}Mn_{1/3}O_2$. Chin Sci Bull, 2010, 55: 2520–2522
26 Li J G, He X M, Zhao R S. Stannum doping of layered $LiNi_{3/8}Co_{2/8}Mn_{3/8}O_2$ cathode materials with high rate capability for Li-ion batteries. J Power Sources, 2006, 158: 524–528
27 Tsutomu O, Atsushi U, Masatoshi N. Electrochemistry and structural chemistry of $LiNiO_2$(R-3m) for 4 volt secondary lithium cells. J Electrochem Soc, 1993, 140: 1862–1870
28 Liu S Q, Li S C, Huang K L. Investigations on the electrode process and kinetics of Li-ion extraction/insertion in $Li_3V_2(PO_4)_3$. Acta Chim Sinica, 2007, 65: 10–16
29 Zhuang Q C, Xu J M, Fan X Y. The research of electrochemical impedance spectroscopy for ion transport characteristics in $LiCoO_2$ battery anode materials. Chin Sci Bull, 2007, 52: 147–153
30 Lee D J, Scrosatia B, Sun Y K. $Ni_3(PO_4)_2$-coated $Li[Ni_{0.8}Co_{0.15}Al_{0.05}]O_2$ lithium battery electrode with improved cycling performance at 55°C. J Power Sources, 2011, 196: 7742–7746